energies

MDPI

Article

DE-Algorithm-Optimized Fuzzy-PID Controller for AGC of Integrated Multi Area Power System with HVDC Link

Solomon Feleke [1], Raavi Satish [2], Workagegn Tatek [1], Almoataz Y. Abdelaziz [3] and Adel El-Shahat [4,*]

[1] Department of Electrical and Computer Engineering, DebreBerhan University, DebreBerhan 445, Ethiopia
[2] Department of Electrical & Electronics Engineering, Anil Neerukonda Institute of Technology and Science (A), Visakhapatnam 531162, India
[3] Faculty of Engineering and Technology, Future University in Egypt, Cairo 11835, Egypt
[4] Energy Technology Program, School of Engineering Technology, Purdue University, West Lafayette, IN 47906, USA
* Correspondence: asayedah@purdue.edu

Abstract: A power system's nonlinearity and complexity increase from time to time due to increases of power demand. Therefore, properly designed power system controlsare required. Without these, system instability will cause equipment failures, and possibly even cascading events and blackouts. To cope with this, intelligent controllers using soft computing are necessary for real time operation. In this paper, the reheat type three-area thermal power system is considered, and the output scaling factors, gain parameters of fuzzy membership functions, and parameters of fuzzy-proportional integral derivative (FPID) controllers are optimized using a differential evolution (DE) optimization techniqueand integral time multiplied absolute error (ITAE) as objective functions. To improve the limitations of the controller and to enhance stability of the system, high voltage direct current (HVDC) technology is advantageous due to its quickresponse capabilities. In this paper, a HVDC is connected in parallel to the system, revealing that a FPID controller with a HVDC provides better and more accurate resultscompared to a system without a controller. The test results presented in this paper show the proposed controller's suitability for managing random load changes.

Keywords: AGC; area control error; fuzzy; PID; differential evolution; HVDC

Citation: Feleke, S.; Satish, R.; Tatek, W.; Abdelaziz, A.Y.; El-Shahat, A. DE-Algorithm-Optimized Fuzzy-PID Controller for AGC of Integrated Multi Area Power System with HVDC Link. *Energies* **2022**, *15*, 6174. https://doi.org/10.3390/en15176174

Academic Editors: Feng Liu, Zhi-wei Liu, Ming Chi and Ming-Feng Ge

Received: 9 July 2022
Accepted: 17 August 2022
Published: 25 August 2022

1. Introduction

1.1. Background and Motivation

In order to continuously supply electricity to customers, there is a need to configure different generators together. Due to load changes at the customers' sites, the reactive power increases, the voltage drops, and the demand for active power increases. This leads the frequency of the supply to decrease. This change in frequency will affect customers' plant production processes. As a consequence, this will decrease the economic outputof the generation companies and the productivityof the customers. To operate all generators at the desired speed, and to interconnect them together, the entire system must be properly controlled. Thus, acceptable frequency and power control devices should be provided for each generator. To realize effectivesystem design, it is necessary to select a proper optimization technique and to consider the controller design complexity. Considering these challenges, in recent times, there has been substantial attention paidto the application of HVDC in automatic generation control(AGC) for the damping of power oscillation. In this paper, the simplest and most efficient method of nonlinear control, DE-algorithm-optimized FPID controller plusa HVDC, is used to overcome the problemsassociated with power and frequency deviation.

1.2. Literature Review

The demands and complexities of the world's power systemsare increasing daily due the increasing population size, the development of emerging new technologies, and the increase of industrialization and automation systems. Automatic generation control (AGC) is the one of many different power system control methods. There are different methods of power system control that adjust the power output of interconnected generators in response to changes in load demand in order to keep a system ina steady state.Many works have been done using different artificial intelligent techniques for the tuning of PID controllers. In [1], a fuzzy logic controller (FLC) with GA was designed for the AGC of a single area. The proposed GAFLC appeared very powerful, even under load perturbations, and the GA also demonstrated the advantage of avoiding local optima.The authors of [2] provide a comprehensive overview of various AGC models in diverse power system configurations. In [3], to overcome the large overshoot and reverse regulation for external disturbances, frequency-based segment values of frequency bias for areas under tie-line load and frequency bias control mode are developed considering multi-dead band effects. The authors of [4] propose a scheme of controller and optimization technique for a two-area system with a diversely sourced power system with various operation time non-linearities such as dead-bands, generation rate constraints, and the reheating of thermal units. In [5], a whale-optimized FPID controller is proposed for managing AGC in multiple-area electrical energy systems with an availability-based tariff-pricing scheme. The authors of [6] propose a teaching–learning-based optimization (TLBO)-tuned FPID controller of two-area hydro-thermal generating units for AGC by considering governor dead band non-linearities and physical constraints. The authors of [7] propose the computation of robust supplementary controller type H∞ based on low-order power system models, obtained by application of an N4Sid identification technique, to be installed at the voltage source converter stations of a HVDC link to dampen the electromechanical weak modes. In [8], to enhance load frequency control (LFC) and AGC in a multi-area power system, HVDC-line is proposed to prevent the disaster of a power stability problem and the loss of synchronism. In [9], a FPID controller for the AGC of a multi-area power system using a GWO algorithm is proposed. The robustness of the proposed controller is tested on sinusoidal and random step load patterns. The authors of [10] deal with an optimal hybrid FPID controller optimized by a hybrid DE-GWO algorithm for the AGC of an interconnected multi-source three-area, interconnected thermal, hydro, and gas power system. Better dynamic performance was achieved by the proposed controller in terms of peak overshoot, settling time, and peak undershoot. In [11], the author addresses a new decentralized fuzzy logic-based LFC scheme for the simultaneous minimization of system frequency deviation and tie-line power changes, which is required for the successful operation of interconnected power systems in the presence of high-penetration wind power. Because the presence of wind power in a system imposes additional power imbalances, which increase the deviation of the frequency from normal. The authors in [12] proposed an improved ant colony optimization algorithm. An optimized FPID controller is proposed for LFC of multi area systems. The nonlinear incremental evaporation rate and improvement of pheromone increment updating are proposed in the algorithm to improve the quality of solution. Additionally, modified objective functions using ITAE, overshoot, undershoot, and settling time with appropriate weight coefficients is discussed to improve the performance of the controller. In [13], a novel cascaded PD-FPID controller is proposed for a conventional hybrid-source unified power system for AGC. The optimization of the scaling parameters of the suggested PD-FPID controller is done by a hybrid GWO-TLBO technique.

The design problems of the DE-algorithm-optimized FPID controller have gained attention, therefore, various control techniques have been reviewedfor the AGC of an integrated multi-area power system design, including [14] the proposal of a new optimization method called flower pollination algorithm for the robust tuning of a static VAR compensator in order to mitigate power system oscillations. It discussed the optimization technique of damping the controller to design a static VAR compensator for AC transmis-

sion. In [15], an artificial cuckoo search algorithm for the optimal tuning of proportional integral controllers for load frequency control is proposed. The PI controller parameter tuning using an artificial Cuckoo test in different conditions is considered. The controller is linear and the system is highly nonlinear; the author didnot check the control performance againstthe system nonlinearity. The authors [16] propose an optimal FPID controller for LFC designed by a proposed mine blast algorithm approach for multi-interconnected areas by considering the nonlinearity of the governor during the dead zone. The authors of [17] studied the performance of a three-area solar–thermal–wind hydro-system equipped with a fractional order PID-based LFC tuned by various modern metaheuristic optimization algorithms. Such a system has been compared to classical PID-LFC controllers. In [18–21], new control strategies are proposed, which can be extended to an interconnected system.

This paper proposes an optimal tuning of FPID control parameters for an integrated three-area reheat thermal power system with a HVDC link. The parameters of the controller are optimized using a DE-optimization algorithm. The rest of the paper is organized as follows. The materials and methods are discussed in Section 2. The results of the test studies are presented in Section 3. Section 4 presents the discussions. The concluding highlights of the paper are described in Section 5.

1.3. Contributions

- Designinga three-area reheat thermal-interconnected system.
- Proposing five membership functions in a FPID controller for the AGC of a three-area interconnected power system.
- Developing a HVDC-link controller model.
- Incorporating HVDC technology with FPID.
- Optimizing the controller-gained parameters and fuzzy scaling parameters.
- Proposing the optimal location of a HVDC for best dynamic support.
- Approving the successful strength of the proposed controller for random load change.
- Damping of power oscillation using the proposed controller.
- Effectively testing the dynamic improvement of the system from an uncontrolled to a controlled state.

2. Materials and Methods

Figure 1 shows the three-area reheat thermal power plant in an interconnected system with a HVDC link in area 2 and area 3 [22,23]. The power rating of each area is considered as 2000 MW. In a multi-area power system, the secondary control can maintain not only the frequency, but also control the tie-line power flow deviation. To control them, a fuzzy PID controller optimized by DE is proposed to tune the parameters. The membership functions, i-th area control errors are the inputs and u1, u2, and u3 are the outputs for area 1, area 2, and area 3, respectively.

2.1. Controller Structure

Figure 2 shows the FPID controller. K1 and K2 are the inputs and K3 and K4 are the outputs for area 1. Similarly, K5 and K6 are the inputs and K7 and K8 are the outputs for area 2. For area 3, K9 and K10 are the inputs and K11 and K12 are the outputs.

The two inputs employed in the fuzzy controller are error (e) and derivative of error (de or $e^{\cdot}$).The five triangular membership functions of fuzzy linguistic variables applied in this paper for inputs and output from right to left are positive big (PB), positive small (PS), zero (Z), negative small (NS), and negative big (NB). The triangular membership function has the advantage of fast and best response, used to reduce computational burden and to reduce overshoot or undershoot. In the present work, aMamdani-type fuzzy inference engine has been used. The triangular membership function of optimal points has been obtained by a tuning DE optimization method. The output of the FLC is determined by applying a method called center of gravity of defuzzification [24].

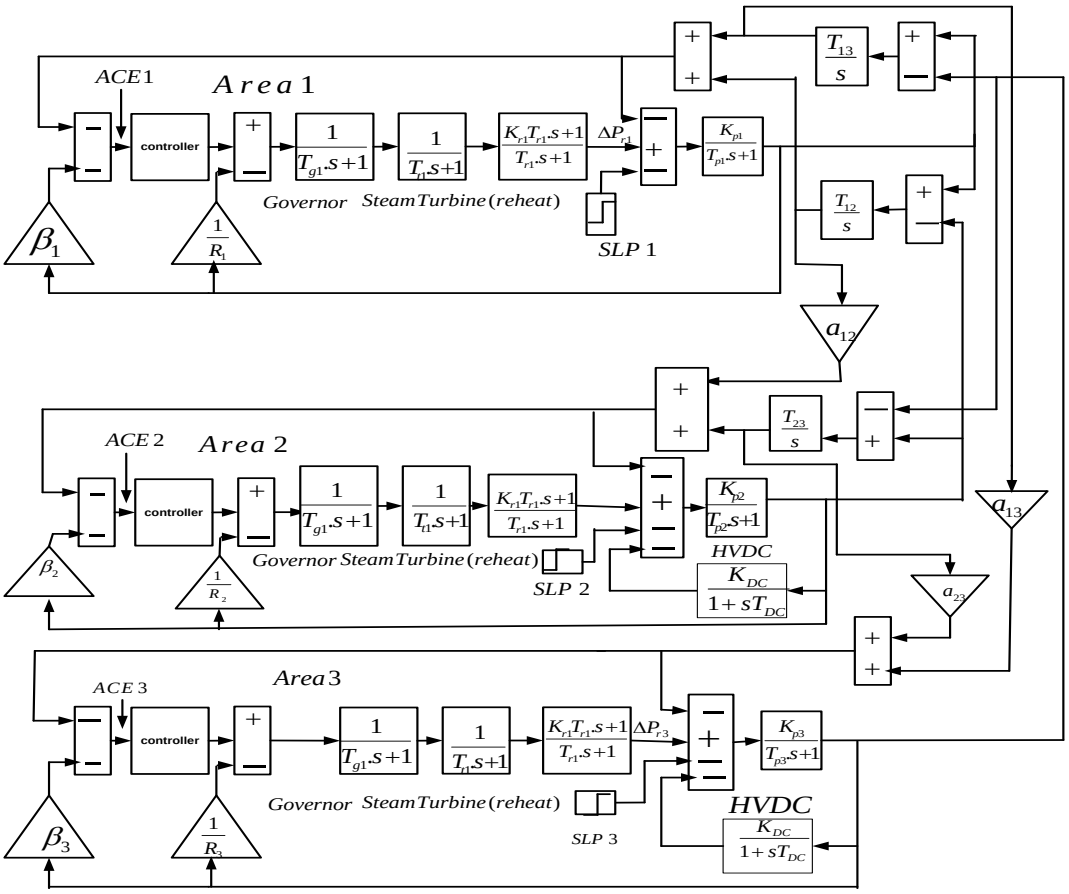

Figure 1. Three-area interconnected thermal power system with an HVDC link in area 2 and area 3.

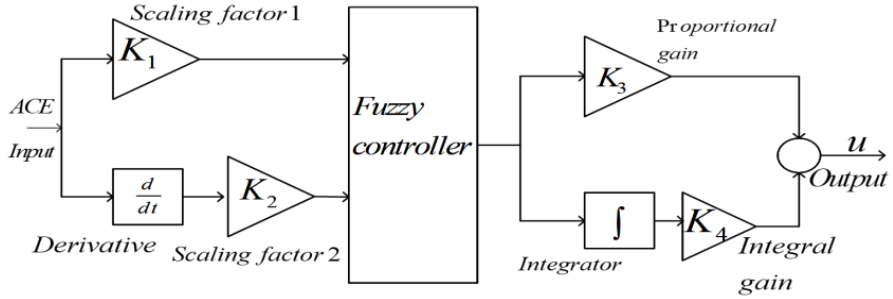

Figure 2. Proposed fuzzy PID controller structure.

Fuzzy Logic Controller

Unlike traditional controllers such as PID controllers, the fuzzy logic controller can act asa solution for a wider range of operating conditions.It consists of fuzzification, knowledge base, fuzzy inference, and defuzzification processes. Fuzzification is used to process a crisp input value to a fuzzy value; knowledge base used to link through the use of rules to their output;the fuzzy inference process is used to formulate a mapping from input to output; and defuzzification is used to transfer a fuzzy inference result into a crisp output [25].

All the fuzzy rules are designed using the connection and are given aweight of 1. As an example, among the twenty-five rules, the first three rules are presented as follows:

1. If (e is NB) and (de is NB) then (u is NB) (1)
2. If (e is NB) and (de is NS) then (u is NB) (1)
3. If (e is NB) and (de is Z) then (u is NS) (1)

2.2. Modeling of HVDC for AGC

Under normal operating conditions, the small frequency deviations can be attenuated by the governor, which is the primary control developed by the natural autonomous response. For large frequency deviations, the LFC, which is the secondary control, is responsible. The application of a control technology for processes such as optimization, intelligent controllers like fuzzy have been applied for power system control to improve the function and performance of the system during normal and abnormal conditions. Furthermore, the function of the AGC can also be improved by interconnecting the HVDC link in parallel with the system.Thus, the HVDC device components and their placement in the power system under study are given in Figure 3 [26,27].

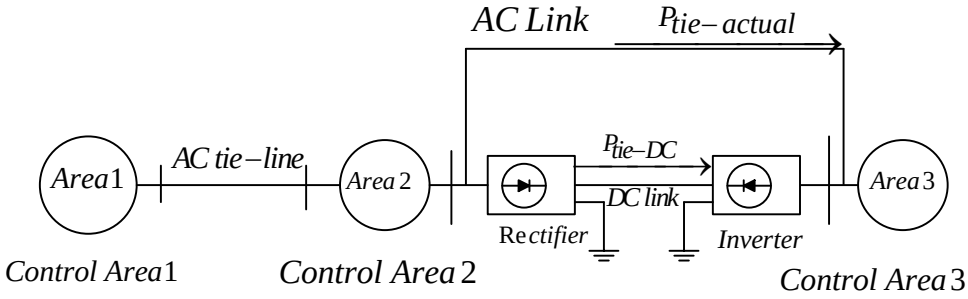

Figure 3. HVDC link connected in area 2 and area 3.

Equation (1) is the description of the HVDC–DC tie-line power model using the first order transfer function [26,27].

$$\Delta P_{tie,DC} = \frac{K_{DC}}{(1 + T_{DC}s)} \tag{1}$$

where, $\Delta P_{tie,DC}$ is the change in *DC* tie-line flow, T_{DC} is the time required by the HVDC, which is used to set the *DC* current during the load perturbation in the interconnected power system. K_{DC} refersto the gain value for the HVDC model.

2.3. Objective Function

For designing the fuzzy PID controller, the ITAE given in Equation (2) is used as the objective function in this paper. This is because, when compared to ITSE, the smaller output provided during the sudden change is the set point, and it reduces the settling time and peak overshoot [28].

$$\text{ITAE} = \int_0^t t|\text{ACE}_i|dt \tag{2}$$

In Equation (2), ACE is a suitable linear combination of frequency and tie-line power changes for *i*-th area [29]. The ACE is given in Equation (3).

$$\text{ACE}_i = \Delta P_{tie,i} + \beta_i \Delta f_i \tag{3}$$

where, $\Delta P_{tie,i}$ and Δf_i are the change in AC tie-line power and the change in frequency for *i*-th area, respectively, whereas β_i is named as a bias factor and can be computed using Equation (4), and it is a combination of the *i*-th droop characteristic (R_i) and *i*-th damping coefficient (D_i)

$$\beta_i = \frac{1}{R_i} + D_i \tag{4}$$

2.4. Differential Evolution Algorithm

The DE algorithm is a search heuristic algorithm [30]; it has the advantage of keeping diversity in the population.The reason behind this is because the mutation and crossover

states in DE support the generation of offspring, which areinvolved in exploring the local search. Furthermore, DE also has the advantages of simplicity, robustness, reliability, speediness, efficiency, and real coding, which help to solve problems in real-type optimization parameters. The four evolutionary operator steps of DE are briefly explained in the following sections [24,30].

2.4.1. Initialization

The first step in DE is the initialization of the parameters. These initial values are taken randomly and uniformly from two interval boundary points known as the lower and upper bounds, which are respectively expressed as: $\left[X_j^L, X_j^U\right]$.

2.4.2. Mutation Operation

In mutation operation, an offspring is produced by combining the target vector, which is commonly known as the trial vector, with the donor vector. Its mathematical expression is given here as:

$$V_{i,G+1} = X_{r1,G} + F(X_{r2,G} - X_{r3,G}) \tag{5}$$

where, F is a scaling factor ranging from (0, 2), G is generation, and the indices r_1, r_2, and r_3 are mutually different, randomly generated integer values. The $V_{i,G}$ is given by:

$$V_{i,G} = \{V_{1i,G}, V_{2i,G}, \cdots V_{Di,G}\}$$

Similarly, D is dimension, which represents individual vector solutions or control variables, and NP is population size, ranging from [1, NP].

2.4.3. Crossover Operation

The crossover, which is the third phase of DE operation used to enhance the potential diversity of the population, and the trial vector (Ui,G+1), can be obtained from the mutant vector (Vi,G) and the target vector (Xi,G). The crossover probability expression is presented in Equation (6). The crossover selected in this paper is 0.98.

$$U_{j,i,G+1} = \begin{cases} V_{j,i,G}, \ if\left(rand_j[0,1] \le CR\right) \ or \ (j = j_{rand}) \\ X_{j,i,G}, otherwise \end{cases}, \ j = 1, 2, \ \ldots, D \tag{6}$$

2.4.4. Selection Operation

The main task in the selection process is to keep the size of the population constant over a subsequent generation. Therefore, to make this happen, a comparison of the target vector $f(X_iG)$ and the trial vector $f(U_iG)$ is performed, and the one that fits best will be selected for the next generation.

$$X_{i,G+1} = \begin{cases} U_{i,G}, if \ f(U_{i,G}) \le f(X_{i,G}) \\ x_{i,G}, \text{otherwise} \end{cases} \tag{7}$$

where, $i \in [1, N_p]$.

The flowchart of the DE algorithm is presented in Figure 4.

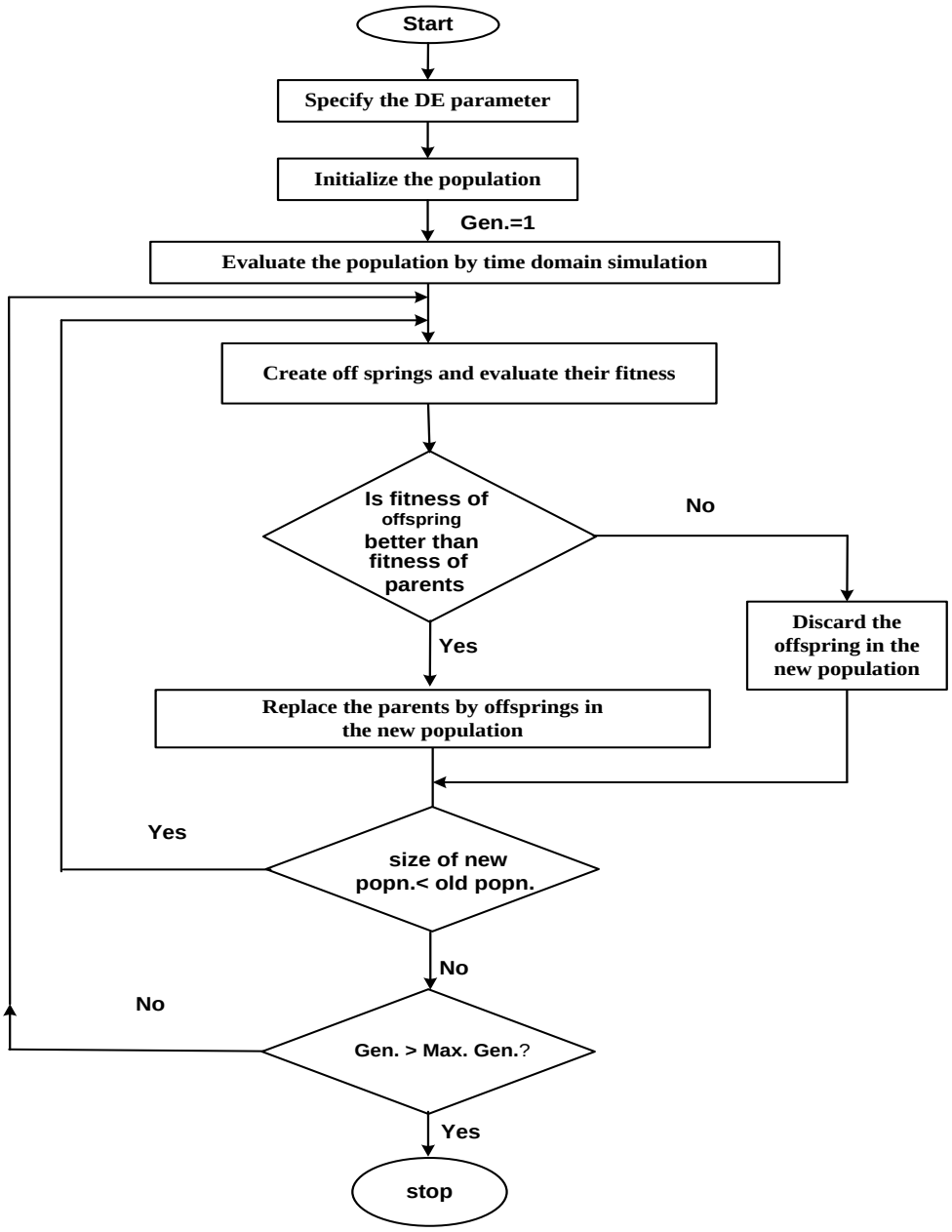

Figure 4. Flow chart of DE optimization.

3. Simulation Results

Three equal-area power systems, which have a total power of 2000 MW in each area, with 0.1, 0.01, and 0.2 p.u. step load changes in area 1, area 2, and area 3, respectively, are applied for dynamic performance. The parameters used for the simulation of the power plant model are presented in Table 1. The DE optimization technique is employed to optimize the gain of the controller parameters, the HVDC gain controller parameters, and the fuzzy membership function scaling factors. The optimized gain parameters for FPID are presented in Table 2, and the optimized scaling factors for the fuzzy are presented in Table 3. During the initialization of the optimization process, the minimum and maximum range is considered as 1 and 2, respectively. A scaling factor of 0.5, a population size of 50 with a total iteration of 100, and acrossover probability of 0.98 aretaken. The program runs 50 times and displays 50 solutions after each termination. A network optimization configuration check through is used to establish the best HVDC configuration for three-area reheat-type thermal power systems at areas two and three. Since the objective function is minimization,

the minimum value will be taken as the best solution. The comparison is made for without controller and DE-optimized FPID with HVDC for the changes of frequency deviations and area control error, which are depicted in Figures 5–10, respectively.The comparison of without controller plus HVDC in areas 2 and 3 with DE-optimized FPID plus HVDC for changes in tie-line power deviation is also given in Figures 11–13. From the time response analyzed simulation task, a better result was achieved from the DE-optimized FPID with HVDC in settling time, steady state error, overshoot, rise time, and undershoot. The convergence characteristics of DE + FPID + HVDC are given in Figure 14, in which the proposed controller with the presence of HVDC converges at iteration number 49. Similarly, the bar graph depicted in Figures 15–18, respectively, compares rise time, settling time, undershoot, and overshoot, respectively.As shown by the comparison with the proper controller, FPID optimized with DE plus HVDC performs better by damping the oscillation of the power system with lower rise time, settling time, undershoot, and overshoot, respectively, than without controller. To check the strong power oscillation damping nature of the proposed controller, different case studies are considered by incorporating random load changes from 0.01 to 1.00 p.u to the system and time versus change in frequency, change in tie-line power deviation, and change in area control.Error graphs were drawn for different case studies from Figures 19–29, and the results showed that the proposed controller with HVDC damped out the oscillation from the change in frequency, the change in tie-line power, and the change in area controller error after a certain settling time.

Table 1. Parameters used for simulation of the power plant model under study.

Parameters	Symbols	Values
Governor time constant	T_g	0.08s
Turbine time constant	T_t	0.3s
Reheat gain	K_r	0.5
Reheat time constant	T_r	10.0s
Control area gain	K_p	120
Control area time constant	T_p	20s
Frequency bias constant	B_ii = 1,2,3	0.425 MW/Hz
Regulation constant	R_ii = 1,2,3	2.4 Hz/MW
Synchronization time constant	T_{12},T_{13},T_{23}	0.0866
HVDC gain value	K_{DC}	1
Time required by the HVDC	T_{DC}	0.2

Table 2. Optimum gains parameter values of FPID controller with HVDC link.

Area 1			Area 2			Area 3					
K1	**K2**	**K3**	**K4**	**K5**	**K6**	**K7**	**K8**	**K9**	**K10**	**K11**	**K12**
1.9999	1.7699	0.9999	1.9873	1.9999	1.4845	1.9999	1.9573	1.9999	1.9444	1.9444	1.9999

Table 3. Optimized fuzzy scaling factor parameters.

Change in Error (e)	Derivative of Error (de)	Output (u)
−1−1−0.4 −0.1	−1−1−0.4 −0.1	−1−1−0.4 −0.1
−0.4 −0.1 0	−0.4 −0.1 0	−0.4 −0.1 0
−0.0947 0.00529 0.105	−0.1 0 0.1	−0.1 0 0.1
0 0.1 0.4	0 0.1 0.4	0 0.1 0.4
0.1 0.4 1 1	0.1 0.4 1 1	0.1 0.4 1 1

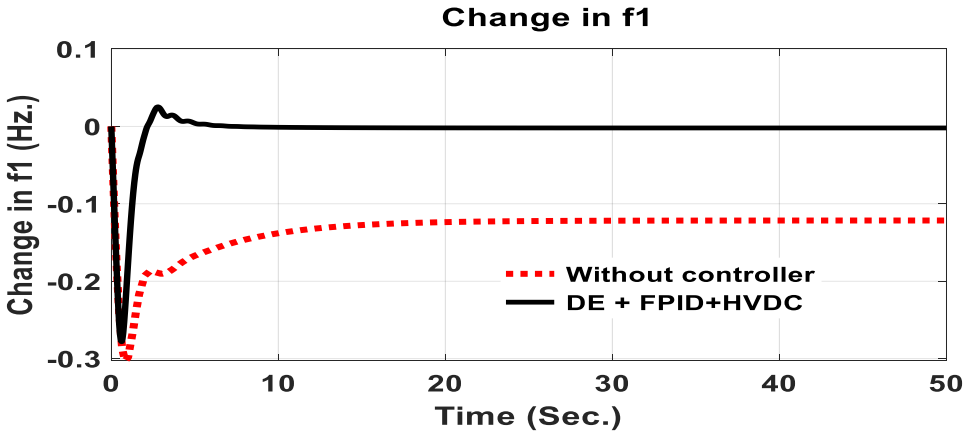

Figure 5. Comparison of controller and without controller for frequency deviation f1.

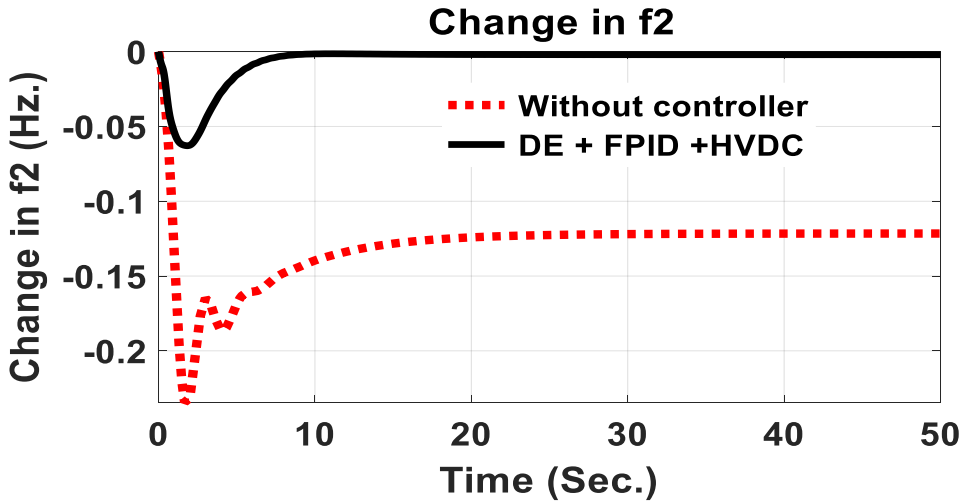

Figure 6. Comparison of controller and without controller for frequency deviation f2.

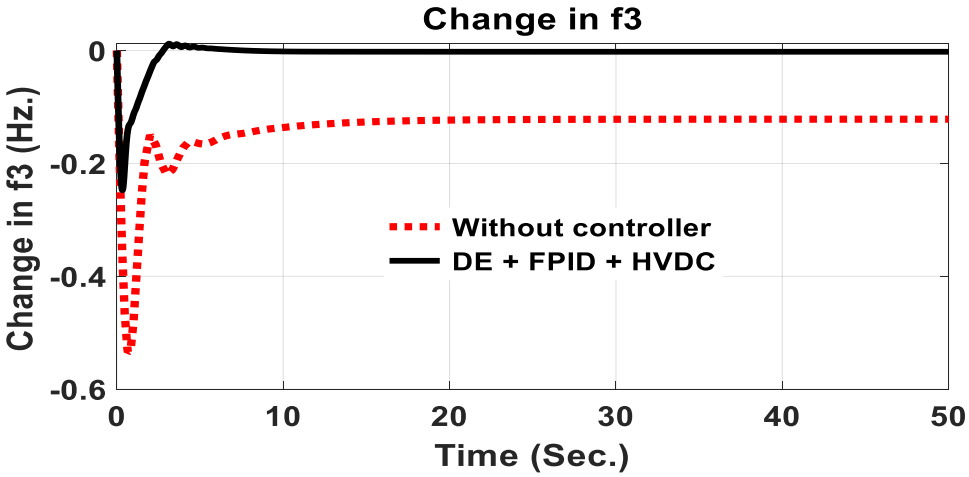

Figure 7. Comparison of controller and without controller for frequency deviation f3.

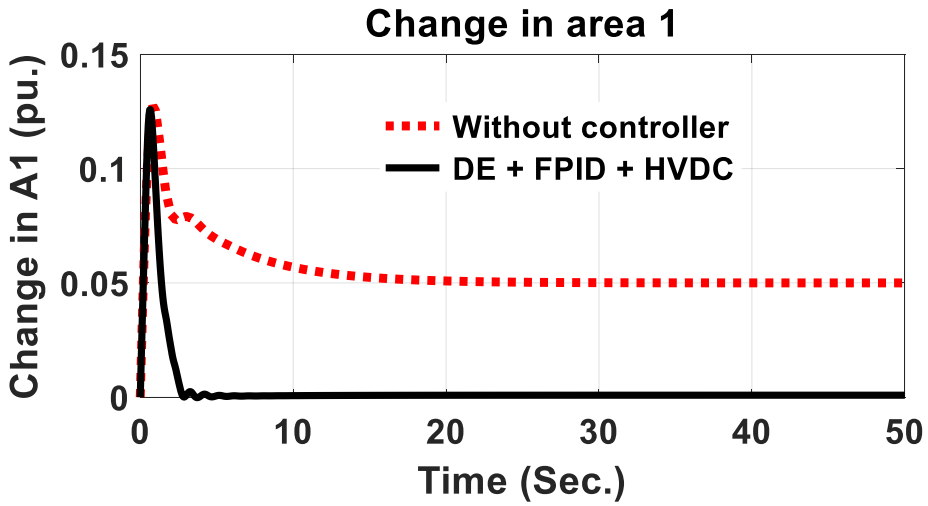

Figure 8. Comparison of controller and without controller for change in ACE 1.

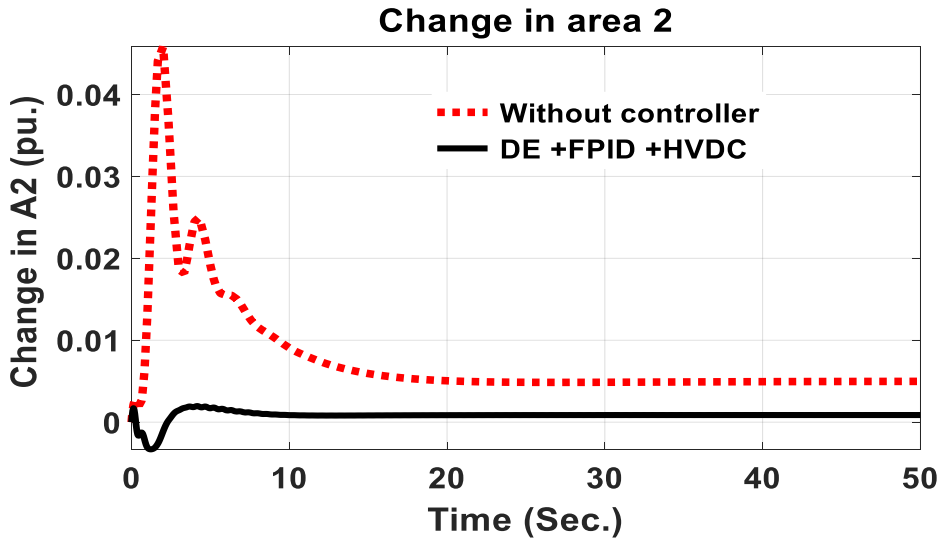

Figure 9. Comparison of controller and without controller forchange in ACE 2.

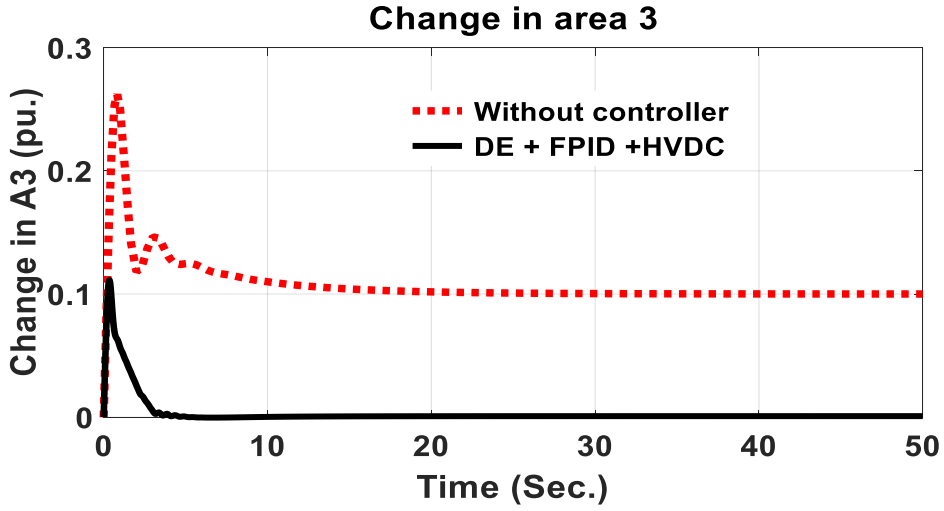

Figure 10. Comparison of controller and without controller for change in ACE 3.

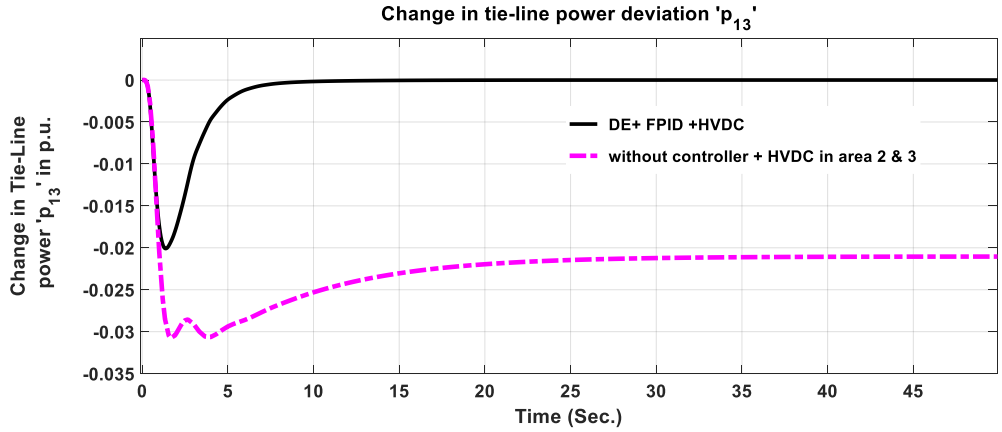

Figure 11. Comparison of controller and without controller + HVDC for change in tie-line power deviation P13.

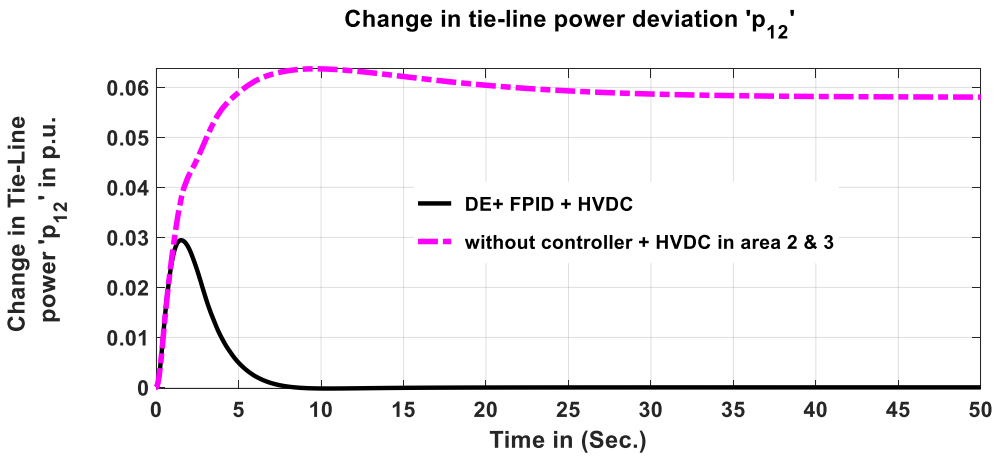

Figure 12. Comparison of controller and without controller + HVDC for change in tie-line power deviation P12.

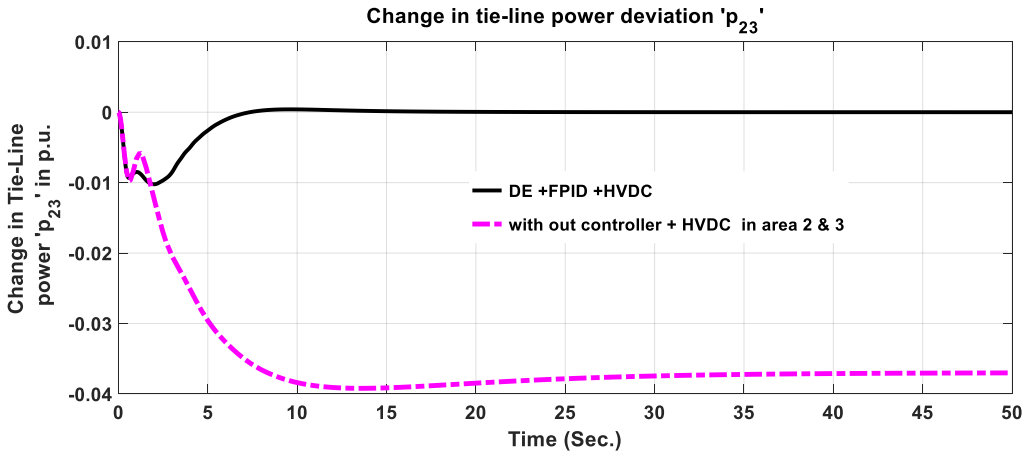

Figure 13. Comparison of controller and without controller + HVDC for change in tie-line power deviation P23.

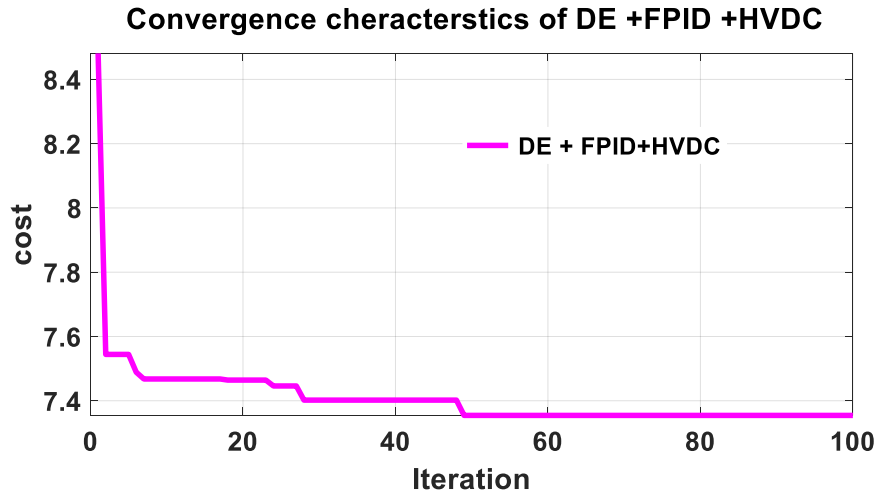

Figure 14. Convergence characteristic for DE + FPID + HVDC.

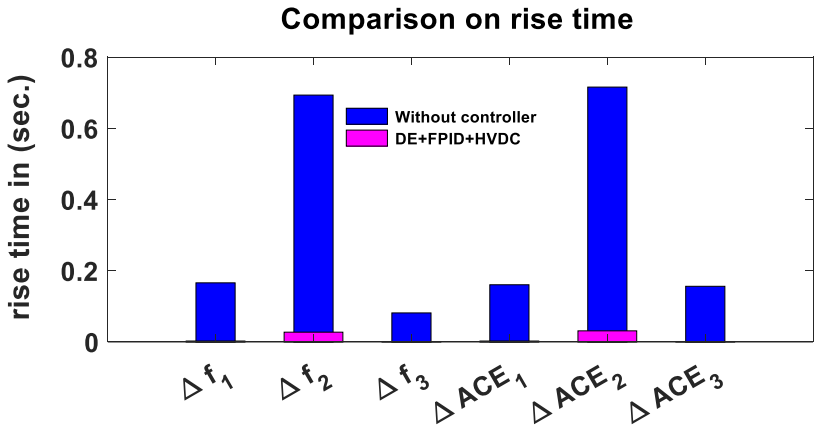

Figure 15. Comparison of controller and without controller for rise time for frequency deviation and area control error.

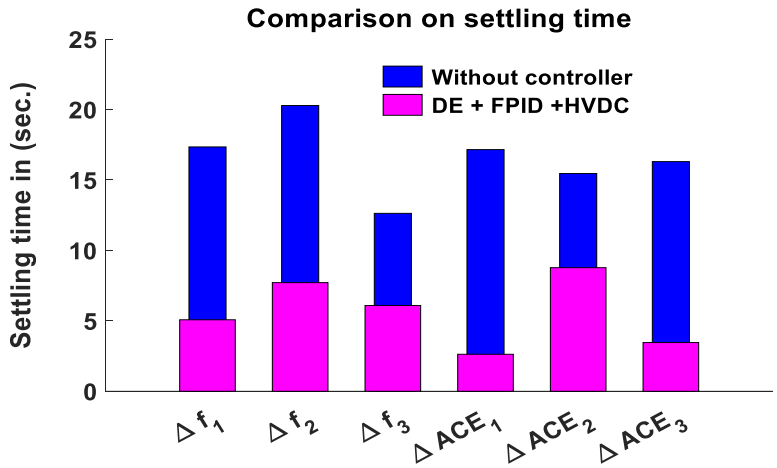

Figure 16. Comparison of controller and without controller for settling time for frequency deviation and area control error.

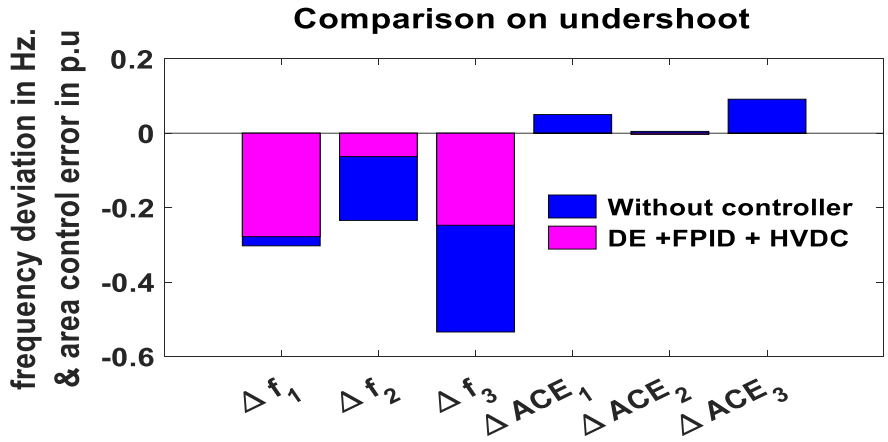

Figure 17. Comparison of controller and without controller for undershoot for frequency deviation and area control error.

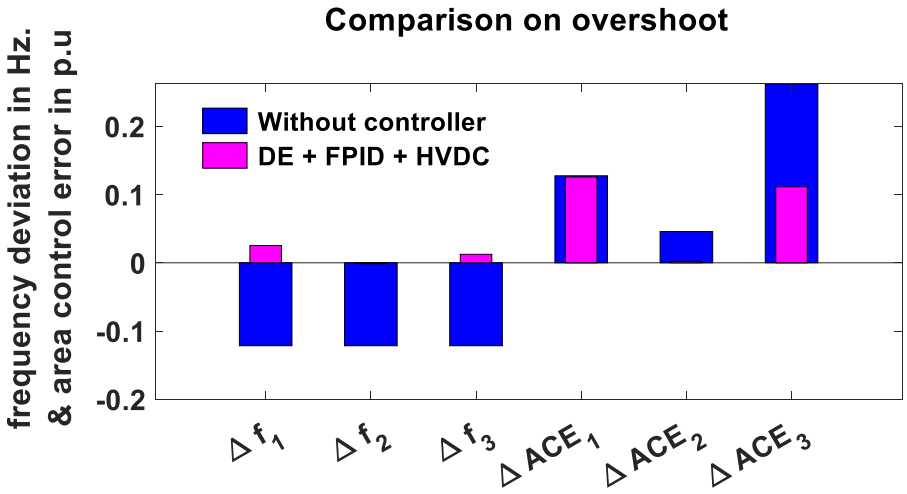

Figure 18. Comparison of controller and without controller for overshoot for frequency deviation and area control error.

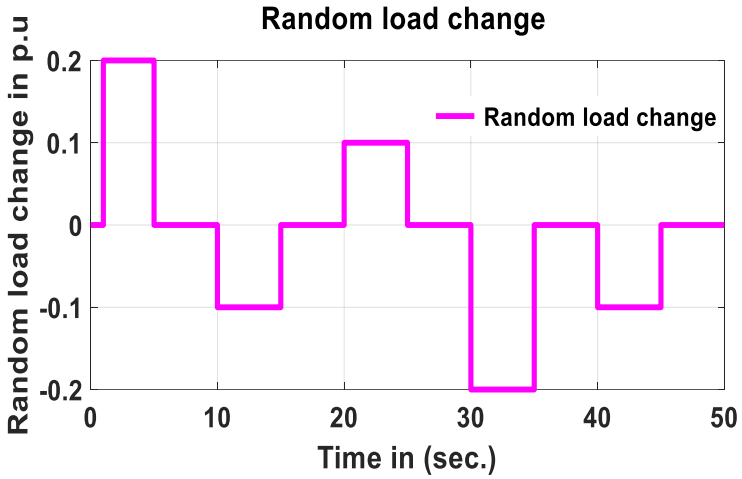

Figure 19. Random load change pattern in the range of [−0.2 to 0.2].

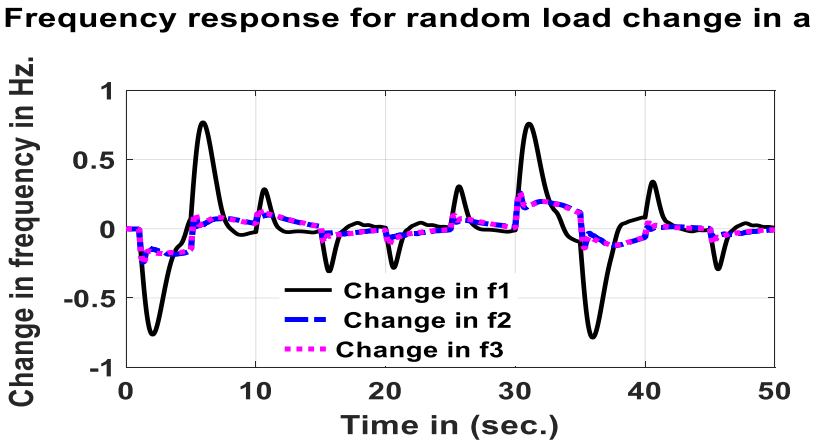

Figure 20. Frequency response of f1, f2 and f3 due to random load change.

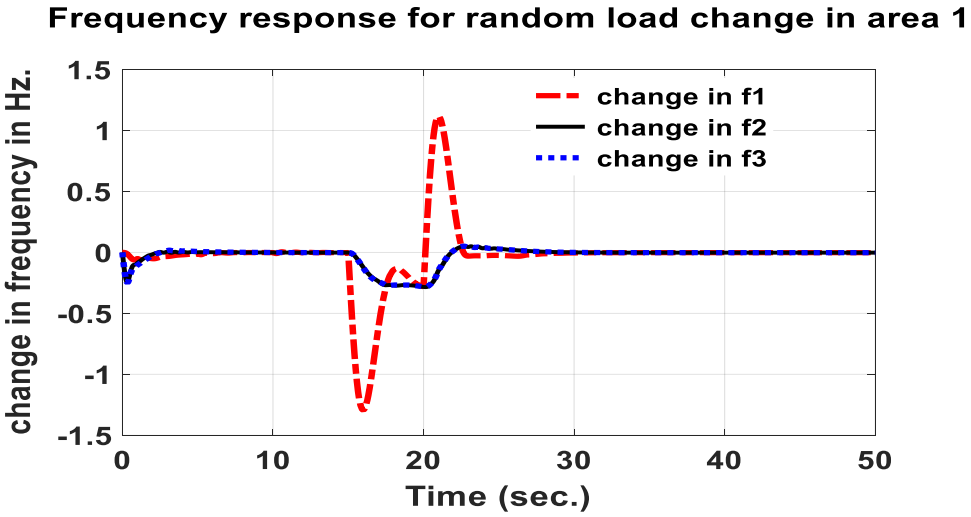

Figure 21. Change in frequency responses of area 1, area 2, and area 3 for random load change in area 1 only.

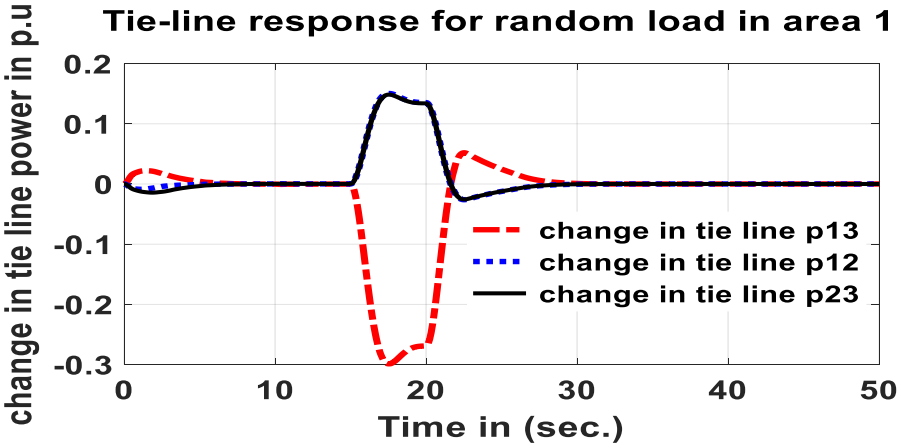

Figure 22. Change in tie-line responses of area 1, area 2, and area 3 for random load change in area 1 only.

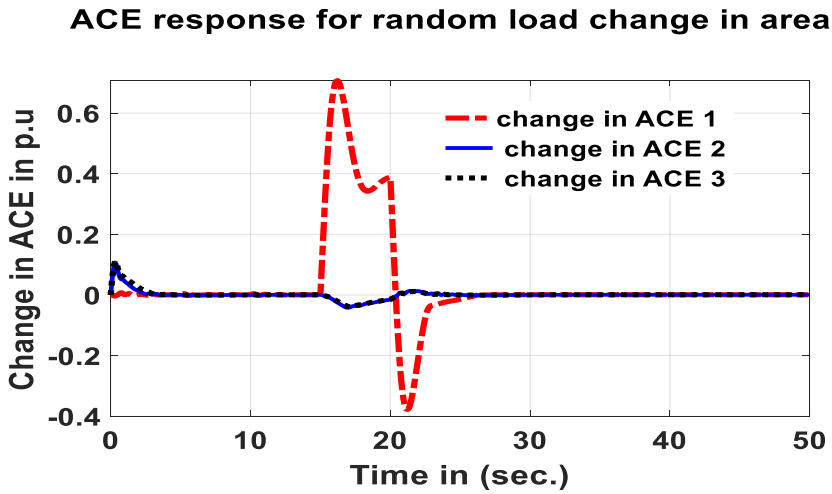

Figure 23. Change in ACE responses of area 1, area 2, and area 3 for random load change in area 1 only.

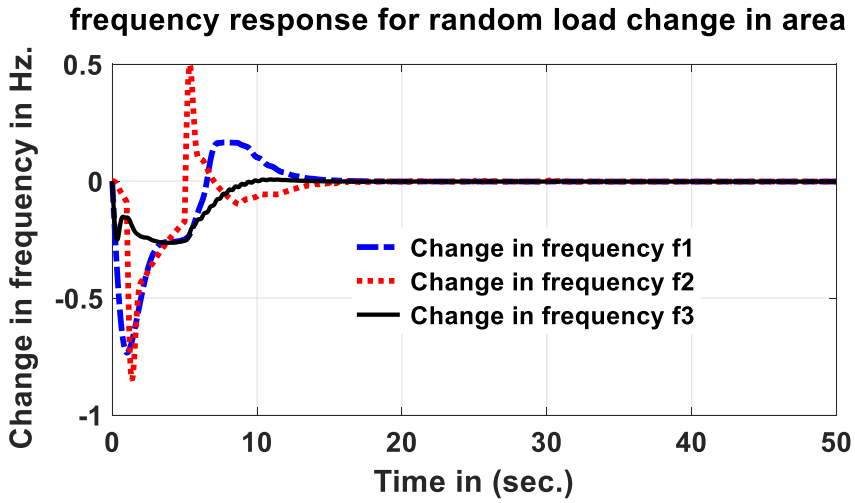

Figure 24. Change in frequency responses of area 1, area 2, and area 3 for random load change in area 2 only.

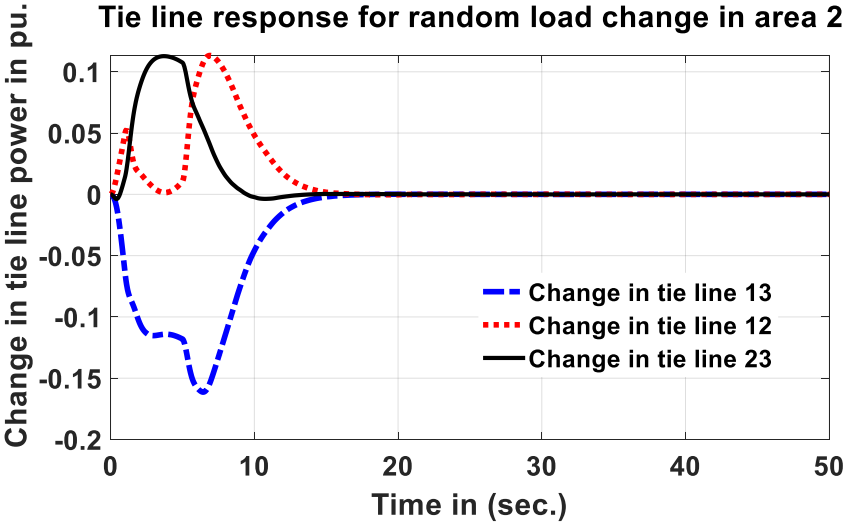

Figure 25. Change in tie-line power responses of area 1, area 2, and area 3 for random load change in area 2 only.

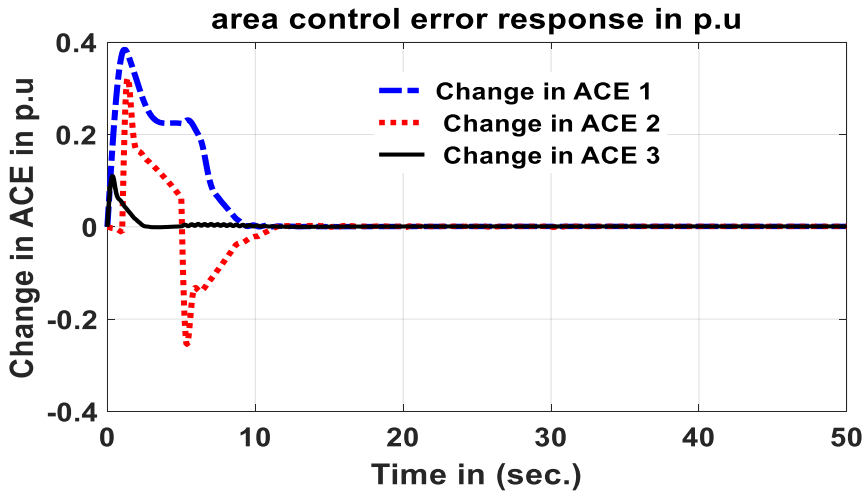

Figure 26. Change in area control error responses of area 1, area 2, and area 3 for random load change in area 2 only.

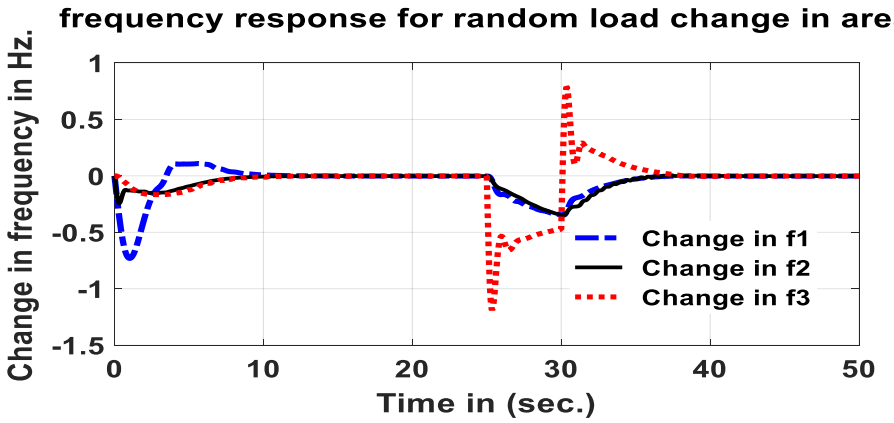

Figure 27. Change in frequency responses of area 1, area 2, and area 3 for random load change in area 3 only.

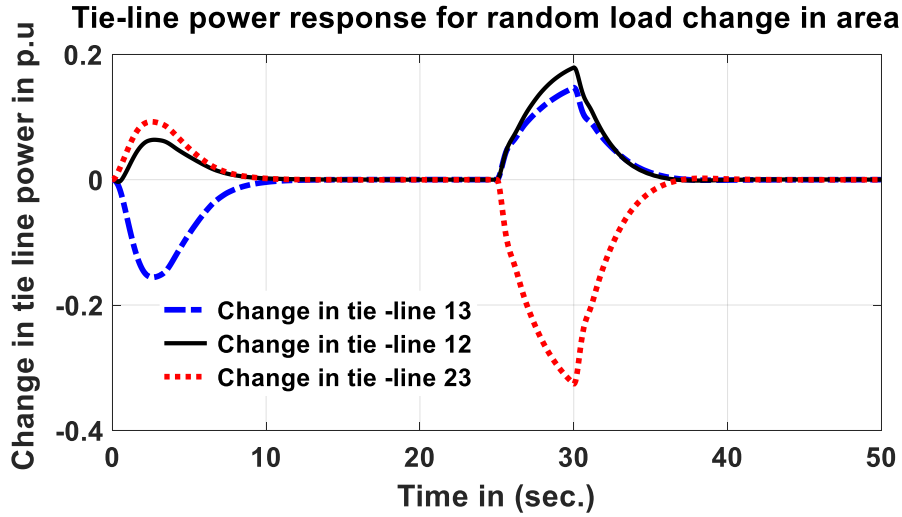

Figure 28. Change in tie-line power responses of area 1, area 2, and area 3 for random load change in area 3 only.

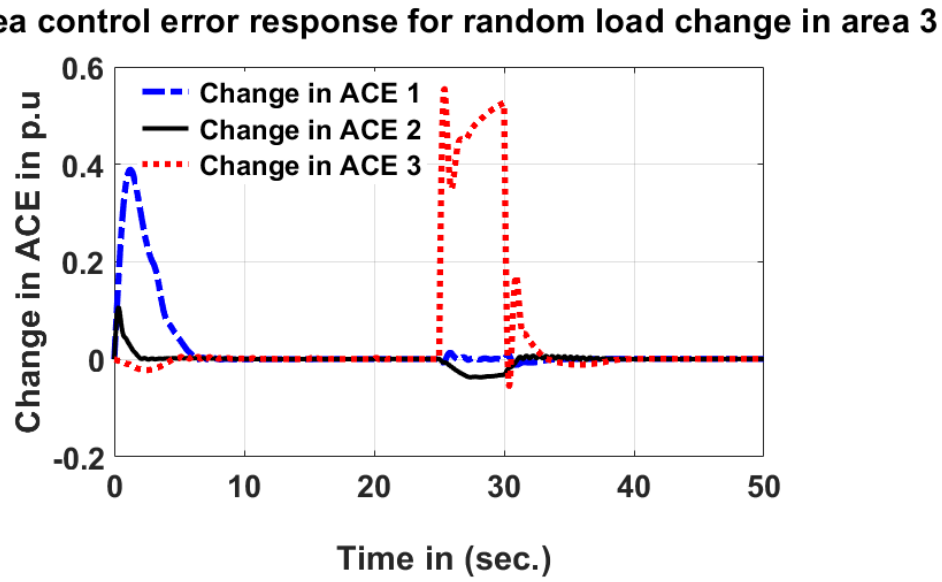

Figure 29. Change in ACE responses of area 1, area 2, and area 3 for random load change in area 3 only.

The objective function used for optimization is ITAE, and as shown bythe results, a smaller error value is obtained in DE-optimized FPID with HVDC, in which an ITAE value of (3.4998) is shown, and for that of without controller, the ITAE value is bigger, which is (187.5810). Time response output values such as rise time, settling time, undershoot, and overshoot for without controller and DE + FPID + HVDC are given in Tables 4 and 5, respectively, for both change in frequency and change in tie-line power deviation, and the results show great improvement from the uncontrolled to the control state. Similarly, the time response performance of AGC for change in tie-line power deviation for without controller with HVDC in areas 2 and 3 and DE + FPID + HVDC are given in Tables 6 and 7, respectively, and the comparison of the two tables shows better AGC performances were achieved with the proposed controller. The ITAE error cost function values for different case studies with controller and without controller are given in Table 8, and they reveal that a lower ITAE error value was obtained from the proposed controller.

Table 4. Transient response of AGC performance evaluation for without controller.

System State Variables	Rise Time	ST	Undershoot	Overshoot
Change in f1	0.1662	17.3468	−0.3028	−0.1216
Change in f2	0.6938	20.2844	−0.2344	−0.1216
Change in f3	0.0817	12.6321	−0.5343	−0.1216
Change in A1	0.1608	17.1556	0.0500	0.1275
Change in A2	0.7163	15.4582	0.0049	0.0458
Change in A3	0.1565	16.3034	0.0914	0.2621

Table 5. Transient response of AGC performance evaluationfor DE+FPID+HVDC.

System State Variables	Rise Time	ST	Undershoot	Overshoot
Change in f1	0.0027	5.0764	−0.2781	0.0253
Change in f2	0.0276	7.7128	−0.0629	−0.0014
Change in f3	0.0014	6.0917	−0.2474	0.0124
Change in A1	0.0027	2.6290	-2.1608×10^{-4}	0.1258
Change in A2	0.0313	8.7746	−0.0033	0.0020
Change in A3	0.0014	3.4587	-3.3680×10^{-4}	0.1114

Table 6. Transient response of AGC tie-line power without controller +HVDC.

System State Variables	Rise Time	ST	Undershoot	Overshoot
Change in P_{13}	0.5344	24.8461	−0.0308	−0.0206
Change in P_{12}	3.0747	25.4990	0.0541	0.0637
Change in P_{23}	6.0143	25.9475	−0.0392	−0.0335

Table 7. Transient response of AGC tie-line power using DE+FPID+HVDC.

System State Variables	Rise Time	ST	Undershoot	Overshoot
Change in P_{13}	0.0012	7.9045	−0.0201	1.0464×10^{-5}
Change in P_{12}	1.5617×10^{-4}	7.2873	-2.2920×10^{-4}	-2.6341×10^{-8}
Change in P_{23}	8.7950×10^{-5}	13.4895	1.6727×10^{-8}	4.0215×10^{-4}

Table 8. ITAE cost function for different loading and controller conditions.

Various Simulation Cases	ITAE Objective Function Value
With FPID controller + HVDC	3.4998
Case 2 random load change in area 2 only	14.6373
Case 1 random load change in area 1 only	61.6618
Random load change in all areas	119.4748
Case 3 random load change in area 3 only	84.1037
Without controller	187.5810

4. Discussion

When random load change was applied to area 1, area 2, and area 3, based on the load change pattern of Figure 19, the frequency response also varied, i.e., when the load initially increases, the frequency decreases, and when the load suddenly drops, the frequency also increases, and vice versa.This frequency response is shown in Figure 20.

4.1. Case 1

Furthermore, to test the efficiency of the controller, three cases have been considered. In case 1, sudden load disturbance is created in area 1 from 0.01, 0.02, 0.03 p.u, and 0.4 p.u SLP for 20 s, keeping the remaining areas, area 2 and area 3, with an SLP of 0.2 p.u.

Figure 21 shows that, when the step load disturbance increases from 0.01 p.u to 0.4 p.u for 20 s, f1 drops with a higher degree than f2 and f3. When the load suddenly drops to zero, the frequencies f1, f2, and f3 are increased; and as time goes on, all the frequencies settle after 26.58 s.

Figure 22 shows that, when the step load disturbance increases from 0.01 p.u to 0.4 p.u for 20 s, the tie-line power p13 drops, while the other tie-lines in the remaining two areas attempt to share the load. When the load suddenly dropped to zero after 20 s, the tie-line power P13 suddenly increased; and finally, as time wenton, all the tie-line power settled after 27.5 s.

As shown in Figure 23, when the step load disturbance increases from 0.01 p.u to 0.4 p.u for 20 s, the ACE in area 1 increases and varies up to the end of 20 s. When the load suddenly dropped to zero after 20 s, the ACE in area 1 suddenly dropped; and finally, as time went on, the ACE in all areas settled after 23.45 s.

4.2. Case 2

A sudden load change or disturbance is created in area 2 from 0.6 p.u to 0.01 p.u for 30 s by keeping an SLP of 0.1p.uinarea 1 and area 3.

A change in load of power demand mainly affects the frequency. As shown in Figure 24, with a higher initial change in load, the frequency suddenly drops, and step-by-step, as load change decreases, the frequency tries to settle after 12.3297 s. Since a higher value of random load change is applied on area 2 as a result, frequency f2 is also more disturbed than f1 and f3.

Similar to frequency, real power also depends on change in load. As shown in Figure 25, initially, the tie-line power (p12) in area 2 drops because of the random load in area 2. As a positive, the other tie powers p13 and p23 tried to share the loads. Step-by-step, the tie-line power settled after 11.8697 s.

The random load change was applied in area 2, which caused more instability for ACE 2 than for ACE 1 and ACE 3, as shown in Figure 26. This big error value in area 2 also affects the frequency stability, as can also be observed in Figure 24. The proposed controller settles ACE after 9.0838 s.

4.3. Case 3

A sudden load change or disturbance is created from 0.01 p.u to 1 p.u for 30 s in area 3 by keeping area 1 and area 2 with 0.2 p.u SLP.

When a big random load change is applied in area 3, the frequency variation in area 3 is also higher thanthe frequency variation in areas 1 and 2. When the load suddenly drops to zero after 30 s, the change in frequency f3 shows a sudden increment, which is shown in Figure 27. After some time, all frequencies start to settle at 35.7043 s. Generally, as the change in load disturbance increases, settling time also increases. This is also clearly observed in the previous random load change demonstrative graphs.

The effect of a random load change in area 3, as shown in Figure 28, affects the tie-line power changes. It is also clearly shown here that, if tie-line power p23 drops, the remaining tie-line powers p13 and p12 share the loads, and after 35.6907 s, the controller settles the system.

It can be observed in Figure 29 that, as step-by-step random load changes increased with time, corresponding to the big load change of 0.9 p.u at time 30 s, the corresponding ACE increases. That is, it affects frequency.To withstand this, other areas will participate to share loads and stabilize the system, settling after 31.3655 s.

5. Conclusions

AGC plays a considerable role in power sharing.When one generator in one area fails or is loaded due to a sudden disturbance, the generators in other areas share the loads to stabilizethe system. In this paper, a DE algorithm is applied to optimize the optimum gain parameter of fuzzy PID controllers. The objective is to make the power system operating condition stable and normal for a three-area reheat thermal power system.The optimization range taken for the simulation is [1.0, –2.0]. This range value was chosen after several trial-and-error tests.

The test results show that a DE-algorithm-based parameter tuning of a FPID controller increases the performance of the transient stability of the network. As shown in Table 5, the change in frequency deviation and the change in area control error with controller plus HVDC is improved. Similarly, the tie-line power deviation is also improved with DE plus FPID with HVDC, as shown in Table 7. Random change in load from 0.01 to 1.0 is applied on the system in different cases or scenarios. And it is concluded that, when load variation increases with steps, it affects the stability of the system, in which it also increases the ITAE error cost function value. However, the proposed controller with HVDC withstands each random load disturbance and damps out system oscillations.

Author Contributions: S.F., R.S. and W.T. the problem under study and performed the simulations and obtained the results. S.F., R.S. and W.T. the paper, which was further reviewed by A.Y.A. and A.E.-S. All authors have read and agreed to the published version of the manuscript.

Funding: This research received no external funding.

Conflicts of Interest: The authors declare no conflict of interest.

Nomenclature

Acronym	Definition
AGC	Automatic generation control
PSS	Power system stabilizer
FPID	Fuzzy proportional integral controller
ITSE	Integral time multiplied square error
ITAE	Integral time multiplied error
UPFC	Unified power flow controller
HVDC	High voltage direct current
ST	Settling time
AVR	Automatic voltage regulator
GWO	Grey wolf optimization algorithm
FACT	Flexible AC transmission
DEPSO	Differential evolution particle swarm optimization
IACO	Improved anti colony optimization
hBFOA	Hybrid bacteria foraging optimization algorithm
DE	Differential evolution
PSO	Particle swarm optimization
SLP	Step load perturbation
ACE	Area controller error
LFC	Load frequency control
IAE	Integral absolute error
ISE	Integral square error
VSC	Voltage source convertor
GA	Genetic algorithm
PV	Photo voltaic
PI	Proportional Integral
PS	Pattern search
AC	Alternating current
DC	Direct current

References

1. Saini, J.S.; Jain, V.A. Genetic algorithm optimized fuzzy logic controller forautomatic generation control for single area system. *J. Inst. Eng. (India) Ser.-B* **2015**, *96*, 1–8. [CrossRef]
2. Ullah, K.; Basit, A.; Ullah, Z.; Aslam, S.; Herodotou, H. Automatic generation control strategies in conventional and modern power systems: A comprehensive overview. *Energies* **2021**, *14*, 2376. [CrossRef]
3. Tan, C.; Li, Y.; Lan, Q.; Xiao, X.; Ding, Q.; Zhang, X.; Wang, M.; Teng, X.; Wang, Y. Multi-Area Automatic Generation Control Scheme Considering Frequency Quality in Southwest China Grid: Challenges and Solutions. *IEEE Access* **2020**, *8*, 199813–199828. [CrossRef]
4. Behera, A.; Panigrahi, T.K.; Ray, P.K.; Sahoo, A.K. A novel cascaded PID controller for automatic generation control analysis with renewable sources. *IEEE/CAA J. Autom. Sin.* **2019**, *6*, 1438–1451. [CrossRef]
5. Hamodat, Z.; Cansever, G. Automated Generation Control of Multiple-Area Electrical System with an Availability-Based Tariff Pricing Scheme Regulated by Whale Optimized Fuzzy PID Controller. *Int. J. Photoenergy* **2021**, *2021*, 5596527. [CrossRef]
6. Pilla, R.; Azar, A.T.; Gorripotu, T.S. Impact of flexible AC transmission systemdevices on automatic generation control with a metaheuristic based fuzzy PID controller. *Energies* **2019**, *12*, 4193. [CrossRef]
7. Laverde, J.S.; Rios, M.A. Damping electromechanical oscillations using supplementary controls at VSC-HVDC stations based on reduced low order models. *Control. Eng. Pract.* **2018**, *79*, 195–208. [CrossRef]
8. Khanjanzadeh, A.; Soleymani, S.; Mozafari, B.; Fotuhi, M. Integrated multi-area power system with HVDC tie-line to enhance load frequency control and automatic generation control. *Electr. Eng.* **2020**, *102*, 1223–1239. [CrossRef]
9. Lal, D.K.; Barisal, A.K. Comparative performances evaluation of FACTS devices on AGC with diverse sources of energy generation and SMES. *Cogent Eng.* **2017**, *4*, 1318466. [CrossRef]
10. Debnath, M.K.; Mallick, R.K.; Sahu, B.K. Application of hybrid differential evolution–grey wolf optimization algorithm for automatic generation control of a multi-source interconnected power system using optimal fuzzy–PID controller. *Electr. Power Compon. Syst.* **2017**, *45*, 2104–2117. [CrossRef]
11. Bevrani, H.; Daneshmand, P.R. Fuzzy logic-based load-frequency control concerning high penetration of wind turbines. *IEEE Syst. J.* **2011**, *6*, 173–180. [CrossRef]

12. Chen, G.; Li, Z.; Zhang, Z.; Li, S. An improved ACO algorithm optimized fuzzy PID controller for load frequency control in multi area interconnected power systems. *IEEE Access* **2019**, *8*, 6429–6447. [CrossRef]
13. Debnath, M.K.; Jena, T.; Mallick, R.K. Optimal design of PD-Fuzzy-PID Cascaded controller for automatic generation control. *Cogent Eng.* **2017**, *4*, 1416535. [CrossRef]
14. Abdelaziz, A.Y.; Ali, E.S. Static VAR Compensator Damping Controller Design Based on Flower Pollination Algorithm for a Multi-machine Power System. *Electr. Power Compon. Syst.* **2015**, *43*, 1268–1277. [CrossRef]
15. Abdelaziz, A.Y.; Ali, E.S. Load Frequency Controller Design via Artificial Cuckoo Search. *Electr. Power Compon. Syst.* **2016**, *44*, 90–98. [CrossRef]
16. Fathy, A.; Kassem, A.M.; Abdelaziz, A.Y. Optimal Design of Fuzzy-PID Controller for Deregulated LFC of Multi-Area Power System via Mine Blast Algorithm. *Neural Comput. Appl.* **2020**, *32*, 4531–4551. [CrossRef]
17. Ebrahim, M.A.; Becherif, M.; Abdelaziz, A.Y. PID/FOPID-based Frequency control of zero-carbon multi-sources based interconnected power systems under deregulated scenarios. *Int. Trans. Electr. Energy Syst.* **2021**, *31*, e12712. [CrossRef]
18. Pang, Z.-H.; Fan, L.-Z.; Sun, J.; Liu, K.; Liu, G.-P. Detection of stealthy false data injection attacks against networked control systems via active data modification. *Inf. Sci.* **2021**, *546*, 192–205. [CrossRef]
19. Pang, Z.-H.; Fan, L.-Z.; Dong, Z.; Han, Q.-L.; Liu, G.-P. False Data Injection Attacks Against Partial Sensor Measurements of Networked Control Systems. *IEEE Trans. Circuits Syst. II Express Briefs* **2022**, *69*, 149–153. [CrossRef]
20. Pang, Z.; Bai, C.; Liu, G.; Han, Q.; Zhang, X. A Novel Networked Predictive Control Method for Systems with Random Communication Constraints. *J. Syst. Sci. Complex.* **2021**, *34*, 1364–1378. [CrossRef]
21. Pang, Z.-H.; Zheng, C.-B.; Li, C.; Liu, G.-P.; Han, Q.-L. Cloud-Based Time-Varying Formation Predictive Control of Multi-Agent Systems With Random Communication Constraints and Quantized Signals. *IEEE Trans. Circuits Syst. II Express Briefs* **2022**, *69*, 1282–1286. [CrossRef]
22. Sahu, B.K.; Pati, S.; Panda, S. Hybrid differential evolution particle swarm optimization optimised fuzzy proportional–integral derivative controller for automatic generation control of interconnected power system. *IET Gener. Transm. Distrib.* **2014**, *8*, 1789–1800. [CrossRef]
23. Nanda, J.; Mishra, S.; Saikia, L.C. Maiden application of bacterial foraging base optimization technique in multi area automatic generation control. *IEEE Trans. Power Syst.* **2009**, *24*, 602–609. [CrossRef]
24. Padhan, S.; Sahu, R.K.; Panda, S. Automatic generation control with thyristor controlled series compensator including superconducting magnetic energy storage units. *Ain Shams Eng. J.* **2014**, *5*, 759–774. [CrossRef]
25. Al-Turki, Y.; Attia, A.-F.; Soliman, H.F. Optimization of fuzzy logic controller for supervisory power system stabilizers. *Acta Polytech.* **2012**, *52*. [CrossRef]
26. Kumar, V.N.J.; Ansari, T.M.M. A new design of dual mode Type-II fuzzy logic load frequency controller for interconnected power systems with parallel AC–DC tie-lines and capacitor energy storage unit. *Int. J. Electr. Power Energy Syst.* **2016**, *82*, 579–598. [CrossRef]
27. Arya, Y.; Kumar, N. AGC of a multi-area multi-source hydrothermal power system interconnected via AC/DC parallel links under deregulated environment. *Int. J. Electr. Power Energy Syst.* **2016**, *75*, 127–138. [CrossRef]
28. Lee, C.-H.; Chang, F.-K. Fractional order PID controller optimization via improved electromagnetism-like algorithm. *Expert Syst. Appl.* **2010**, *37*, 8871–8878. [CrossRef]
29. Bevrani, H. *Robust Power System Frequency Control*, 2nd ed.; Power Electronics and Power Systems; Springer: New York, NY, USA, 2014.
30. Storn, R.; Price, K. Differential evolution–a simple and efficient heuristic for global optimization over continuous spaces. *J. Glob. Optim.* **1997**, *11*, 341–359. [CrossRef]